

P2.28 Evolution of Hurricane-like Eye-wall Structures using a Divergent, Normal-Mode, Spectral Model

Thomas A. Guinn*

Embry-Riddle Aeronautical University, Daytona Beach, FL

1. INTRODUCTION

Improving our understanding of the dynamics of hurricane eye-wall asymmetries may provide valuable insight into the intensification process as well as the formation of meso-vortices. The evolution of the dry dynamics/advective processes associated with hurricane-like eye-wall structures has been widely investigated using non-divergent barotropic models (e.g., Schubert *et al*, 99; Kossin *et al*, 2000; Kossin *et al*, 2001; Kossin and Schubert, 2001; Prieto *et al*, 2001; Hendricks *et al*, 2009). More recently Hendricks *et al* (2010) examined and compared simulations of an unique “off-center” eye-wall structure motivated by radar observations of Hurricane Ivan. In their study they used both a divergent barotropic (shallow-water) model and a non-divergent barotropic model. Their study demonstrated that both the divergent and non-divergent models produced nearly identical results, thus indicating the gravity-inertia modes played a minimal role in the evolution of the vorticity field. In the present study, the evolutions of a variety of hurricane-like eyewall structures are examined using a divergent, barotropic (shallow-water) normal-mode spectral model on an f -plane. The normal-mode solution technique offers the distinct advantage of readily allowing the individual contributions to the total mass and momentum fields from the gravity-inertia (fast) modes and rotational (slow) modes to be partitioned and examined independently. This model was originally developed to examine the evolution of hurricane outer and inner spiral bands (Guinn and Schubert, 1993) (hereafter GS93). However, the studies of GS93 involved relatively low-resolution simulations of artificially large vortex structures necessitated by computational limitations of the day.

This brief paper examines the evolution hurricane-like vortex and eye-wall structures that are more realistic in size and intensity than those considered in GS93, albeit still highly idealized in terms of shape and structure. Specifically this study uses the normal-mode, shallow-water model to replicate and examine the evolution of several initial vorticity patterns that have been explored in previously published works using non-divergent barotropic models. The study first

explores the total solution of the vorticity field in the shallow-water framework to verify the model results are in reasonable agreement with their non-divergent counterparts. Second, the total solution is partitioned into the gravity-inertia and rotational mode contributions at various instances in the time integration to determine the individual contributions of each. Consistent with the lower-resolution simulations of GS93, the contribution to the vorticity pattern by the gravity-inertia modes is nearly negligible compared to the rotational modes. However, the gravity-inertia mode contribution to the wind structure appears to be well correlated with the divergence field, as should be expected.

2. MODEL DETAILS

The unforced shallow water equations on an f -plane can be written in rotational form as:

$$\frac{\partial u}{\partial t} - (f + \zeta)v + \frac{\partial}{\partial x} \left[\varphi + \frac{1}{2}(u^2 + v^2) \right] = \mu \nabla^2 u$$

$$\frac{\partial v}{\partial t} + (f + \zeta)u + \frac{\partial}{\partial y} \left[\varphi + \frac{1}{2}(u^2 + v^2) \right] = \mu \nabla^2 v$$

$$\frac{\partial \varphi}{\partial t} + c^2 \left(\frac{\partial u}{\partial x} + \frac{\partial v}{\partial y} \right) + \frac{\partial(u\varphi)}{\partial x} + \frac{\partial(v\varphi)}{\partial y} = \mu \nabla^2 \varphi$$

The predictive variables are the east-west, north-south components of wind (u, v) and the deviation geopotential height, $\varphi = gh$, where h is the deviation of the fluid depth from its mean value H . The normal-mode solution technique for the shallow-water equations is discussed in detail in GS93 and not addressed here. For the present study, the equations are solved on a 600 km by 600 km doubly periodic domain using 512 by 512 equally spaced collocation points. To minimize aliasing error of quadratically non-linear terms, 170 Fourier modes were kept in the calculations. This yielded an effective resolution of 3.53 km, which represents the wavelength of the highest Fourier mode. The domain size was chosen to be large enough to minimize the effects of gravity-wave reflection from the boundaries but small enough to maintain reasonable resolution. The large domain size also minimizes the magnitude of the background vorticity necessary to drive the area-averaged vorticity to zero (*i.e.*, no net circulation) as required by the periodic boundary conditions of the spectral model. Ordinary diffusion is applied to all three predictive variables with a diffusion

*Corresponding author address: Thomas A. Guinn, Embry-Riddle Aeronautical Univ., Department of Applied Aviation Sciences, 600 S. Clyde Morris Blvd, Daytona Beach, FL 32114. Email: guinnt@erau.edu

coefficient (μ) of $87.6\text{m}^2/\text{s}$. This yielded an e-folding damping time of approximately 60 min for disturbances with a total wave number of 170. A third order Adams-Bashforth scheme was used for the time differencing; however, diffusion was calculated using a simple forward (Euler) time-differencing scheme to minimize computational instabilities. The time-step for all simulations varies between 3-5 s depending on the maximum wind velocity associated with the initial vorticity field. A circular sponge layer is applied to the gravity-inertia modes near the edges of the domain to minimize gravity wave reflection. The undisturbed fluid depth (H) for all simulations is 2,000 m resulting in a pure gravity wave speed ($c \equiv \sqrt{gH}$) of $\sim 140\text{ms}^{-1}$.

The model is initialized by first specifying the desired idealized vorticity pattern. The mass and momentum fields are then determined by solving the non-linear balance equation in spectral space using a standard two-dimensional fast Fourier transform (FFT).

3. RESULTS

Three cases are examined in this study. The cases were chosen to closely resemble the initial conditions of published studies that used non-divergent barotropic models. These include the Ivan-like case examined in Hendricks *et al* (2010), the annular eye-wall shape examined in Schubert *et al* (1999) and Hendricks *et al* (2009), and the elliptical (or Kirchhoff) vortex examined in GS93 and Hendricks *et al* (2010).

3.1 Ivan-like Case

The ‘‘Ivan-like’’ initial vorticity pattern consists of an intense circular region of vorticity surrounded by an off-center elliptical region of vorticity representing a secondary eyewall. Between the two vorticity maxima is a moat of relatively weak but non-zero vorticity. This case closely replicates the vorticity pattern studied by Hendricks *et al* (2010).

The absolute vorticity field of the 48 hr model integration evolved in a very similar fashion to both the divergent and non-divergent integrations of Hendricks *et al* (2010) as shown in Fig 1. In slight contrast, the penta-pole pattern in the present simulation is significantly less well-defined than that of Hendricks *et al* (2010). This, however, is most likely attributed to the coarser resolution used in this study (512 collocation points vs. 1024). In Fig. 2 we show the individual contributions to the absolute vorticity field from the rotational modes (Fig. 2a). The similarity of the total solution to the rotational mode contribution indicates the gravity-inertia modes played a nearly negligible role in

the axisymmetrization process of the vorticity field. The contribution to the vorticity field from gravity inertia modes was nearly three orders of magnitude smaller than the contribution from the rotational modes (not shown). This is also consistent with the findings of Hendricks *et al* (2010). Figure 2b shows the contribution to the fluid depth and the wind field from the gravity-inertia modes, again at $t=2$ hrs. The rotational mode contribution accounts for nearly all the total wind solution with a maximum wind vector of 73ms^{-1} (not shown) while the gravity-inertia mode contribution accounts for less than 3% of the maximum total wind vector. On the other hand, the gravity-inertia mode contribution is almost entirely responsible for the height field. This result is consistent with the findings of Schubert and DeMaria (1985) using an axisymmetric model as well as GS93. It is also of interest to note the strong visual correlation between the gravity-inertia mode contribution to the wind field (Fig. 2b) and the divergence field (Fig. 2c). Despite the small magnitude of the gravity-inertia mode contribution to the wind field, it is nearly entirely responsible for transient gravity waves, as would be expected.

3.2 Annular Eyewall Patterns

In the second experiment, the model was initialized with an annular region of vorticity representing an idealized eyewall similar to Schubert *et al* (1999) and Hendricks *et al* (2009). Using the convention of Hendricks *et al* 2009 to define the annulus, the radii r_1 , r_2 , r_3 , and r_4 were set at 35, 45, 50, and 60 km, respectively. This corresponds to thickness and hollowness parameters of 0.73 and 0.23, respectively. The inner region of vorticity was set to $4.2 \times 10^{-4}\text{s}^{-1}$ while the eyewall vorticity region was set to $3.4 \times 10^{-3}\text{s}^{-1}$. The average vorticity of the eye and wall is $1.8 \times 10^{-3}\text{s}^{-1}$ resulting in a maximum initial wind speed of 48ms^{-1} . Consistent with Hendricks *et al* (2009), Fig. 3 shows the absolute vorticity pattern evolved into a wave number four asymmetry before significant mixing occurred and the system axisymmetrized. By 48 hours the vorticity pattern evolved into a monopole similar to both Schubert *et al* (1999) and Hendricks *et al* (2009). In Fig. 4a the rotational mode contribution to absolute vorticity field at $t=6$ hrs is shown. Once again the contribution to the absolute vorticity field from the gravity-inertia modes is nearly three orders of magnitude smaller than the contribution from the rotational modes (not shown), while the rotational mode contribution is nearly identical to the total solution. This again suggests the gravity-inertia modes played a nearly negligible role in the vorticity mixing and symmetrization process. Again, in similar fashion to the Ivan-like case, there is a strong

visual correlation between the gravity-inertia mode contribution to the wind field and the divergence field (Fig. 4b-c).

3.3 Elliptical Eye Patterns

The elliptical eye pattern was designed to approximate a “Kirchhoff” vortex that has a sharp transition from the maximum vorticity center to the background vorticity. This is in contrast to GS93 where the vortex patch smoothly transitioned from its maximum value to the background value in a Gaussian fashion. The vorticity patch was specified using $\zeta(r') = \zeta_{max}S(r')$, where ζ_{max} is the maximum value of vorticity within the interior of the ellipse, and $S(r')$ is the Hermite shape function defined as $S(r') = (1+3r'^2-2r'^3)$. The Hermite shape function has the desirable property of being unity at $r'=0$ and zero at $r'=1$, while having zero slope at both $r=0$ and $r=1$. The radius parameter, $r' = (r-r_1)/(r_2-r_1)$, provides the non-dimensional distance over which the vorticity smoothly decreases from ζ_{max} to zero. The radius, r , is calculated from $r^2 = (x-x_0)^2 + a^2(y-y_0)^2$, where a is the aspect ratio of the ellipse and (x_0, y_0) defines the center of the model domain. The aspect ratio of the ellipse was chosen to be 0.5, while the distance over which the vorticity transitions from ζ_{max} to zero, *i.e.*, (r_2-r_1) , was chosen to be 10 km. This created a relatively sharp-edged vorticity patch approximating a Kirchhoff vortex (*i.e.*, an elliptical “Rankine” vortex).

Figure 5 shows the 48 hr evolution of the absolute vorticity field. The evolution closely follows the results of both GS93 and Hendricks *et al* (2010). As with the previous two experiments, the partitioning of the absolute vorticity field, fluid depth and wind fields show similar results (Fig. 6a-c). That is, the gravity-inertia-mode contribution to the wind field is small (less than one percent of the maximum total wind vector of 49 ms^{-1} , not shown) but is well correlated (visually) with the divergence field. Likewise, the gravity-inertia mode provides the greatest contribution to the height field.

4. SUMMARY AND CONCLUSIONS

The evolution of three well-published classic hurricane-like eye-wall structures was examined using a normal-mode, shallow-water model. These included an off-set circular eye surrounded by an elliptical annulus of higher vorticity (*i.e.*, the Ivan-like case of Hendricks *et al*, 2010), a circular annulus of vorticity (*e.g.*, Schubert *et al*, 1999; Kossin *et al*, 2000; Hendricks *et al*, 2009), and an elliptical vortex (*e.g.*, Hendricks *et al*, 2010), which have all been studied using non-divergent barotropic models. The shallow-water model used here has two distinct advantages over typical non-divergent,

barotropic models. First, shallow water models allow the propagation of gravity-inertia waves, and second, the normal-mode technique allows the contributions to the mass and momentum fields from both the gravity-inertia modes and the rotational modes to be easily partitioned and independently examined.

In each of the simulations, the absolute vorticity patterns evolved in a remarkably similar pattern to their non-divergent counterparts. In addition, the contribution to the vorticity field by the gravity-inertia modes was typically 2-3 orders of magnitude smaller than the contributions by the rotational modes. This suggests the simpler, non-divergent models capture the evolution of vorticity structures quite adequately in idealized simulations. Similar results were found in GS93 but with much coarser resolution and vorticity patterns that were much larger and weaker than characteristic hurricane structures. Lastly, the transient gravity-wave modes were clearly evident in the divergence pattern, which correlated well with the gravity-inertia mode contribution to the wind field.

5. REFERENCES

- Guinn, T.A., and W.H. Schubert, 1993: Hurricane spiral bands. *J. Atmos. Sci.*, **50**, 3380-3403.
- Hendricks, E.A., W.H. Schubert, R.K. Taft, H. Wang, and J.P. Kossin, 2009: Life cycles of Hurricane-Like Vorticity Rings, *J. Atmos. Sci.*, **66**, 705-722
- _____, W.H. Schubert, S.R. Fulton, and B.D. McNoldy, 2010: Spontaneous-adjustment emission of inertia-gravity waves by unsteady vertical motion in the hurricane core. *Quart. J. Roy. Meteor.Soc.*, **136**, 537-548.
- Kossin, J.P., W.H. Schubert, and M.T. Montgomery, 2000: Unstable interactions between a Hurricane's primary eyewall and a secondary ring of enhanced vorticity. *J. Atmos. Sci.*, **57**, 3893-3917.
- _____, and W.H. Schubert, 2001: Mesovortices, polygonal flow patterns, and rapid pressure falls in hurricane-like vortices. *J. Atmos. Sci.*, **58**, 2196-2209.
- Prieto, R., J.P. Kossin, and W.H. Schubert, 2001: Symmetrization of lopsided vorticity monopoles and offset hurricane eyes. *Quart. J. Roy. Meteor.Soc.*, **136**, 537-548.
- Schubert, W.H., and M. DeMaria, 1985: Axisymmetric, Primitive Equation, Spectral Tropical Cyclone Model. Part I: Formulation. *J. Atmos. Sci.*, **42**, 1213-1224.
- _____, M.T. Montgomery, R.K. Taft, T.A. Guinn, S.R. Fulton, J.P. Kossin, and J.P. Edwards, 1999: Polygonal eyewalls, asymmetric eye contraction, and potential vorticity mixing in hurricanes. *J. Atmos. Sci.*, **56**, 1197-1223.

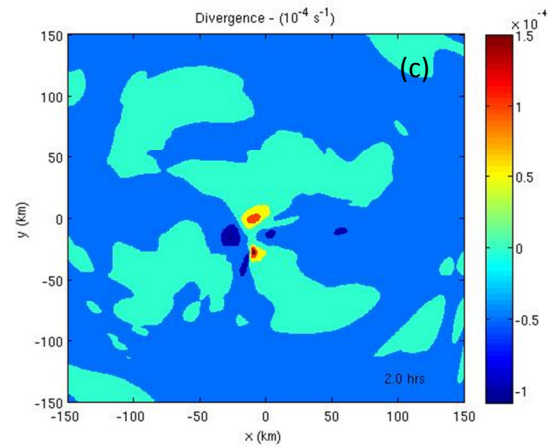
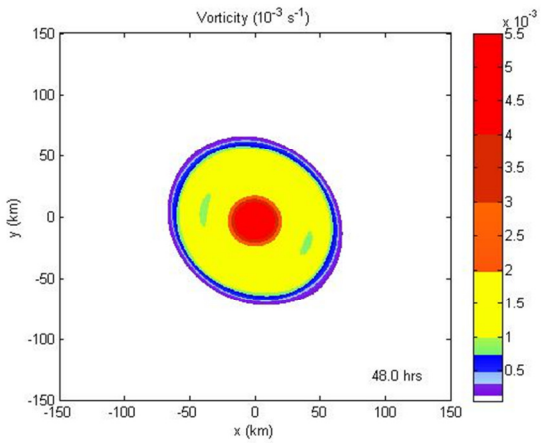
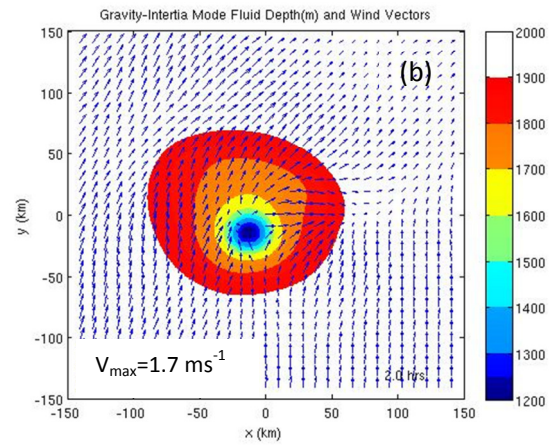
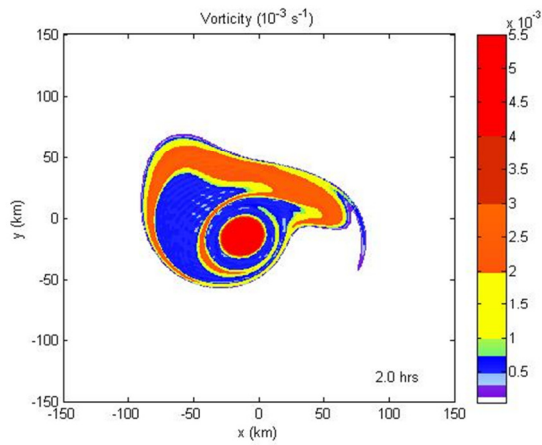
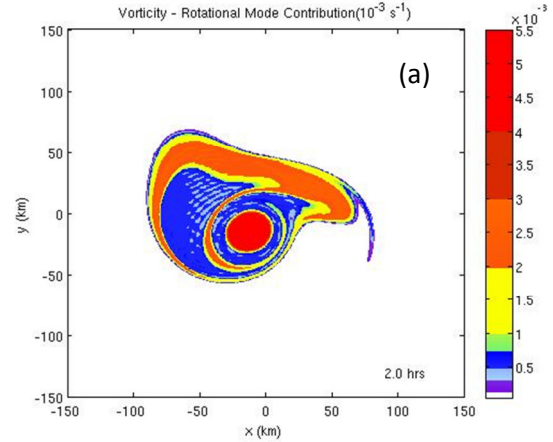
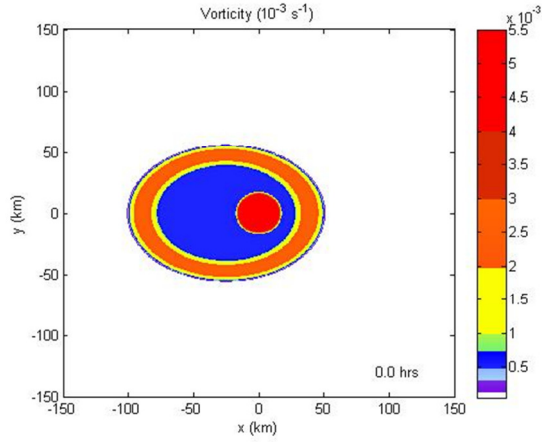


Figure 1: The evolution of the absolute vorticity field at 0, 2, and 48 hours for the "Ivan-like" case.

Figure 2: Various fields for the "Ivan-like" case at 2 hrs. (a) Rotational mode contribution to the absolute vorticity. (b) The gravity-inertia mode contribution to the wind and fluid depth. (c) The divergence field.

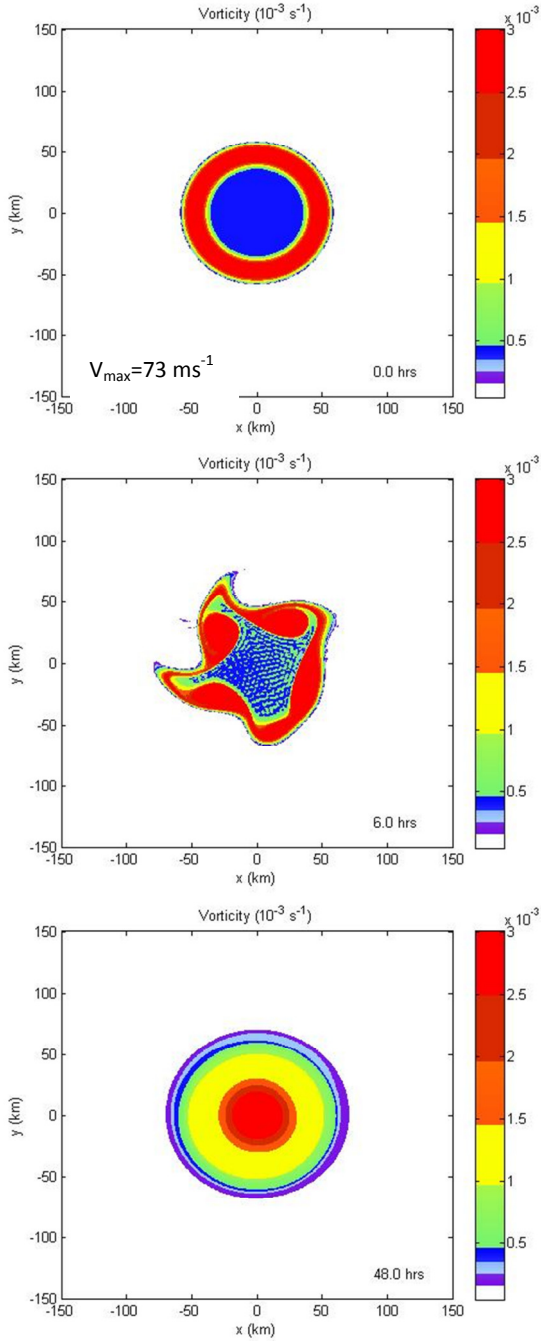


Figure 3: Evolution of the absolute vorticity field for an initial annulus with a hollowness parameter of 0.23 and a thickness parameter of 0.73 at 0, 6, and 48 hours.

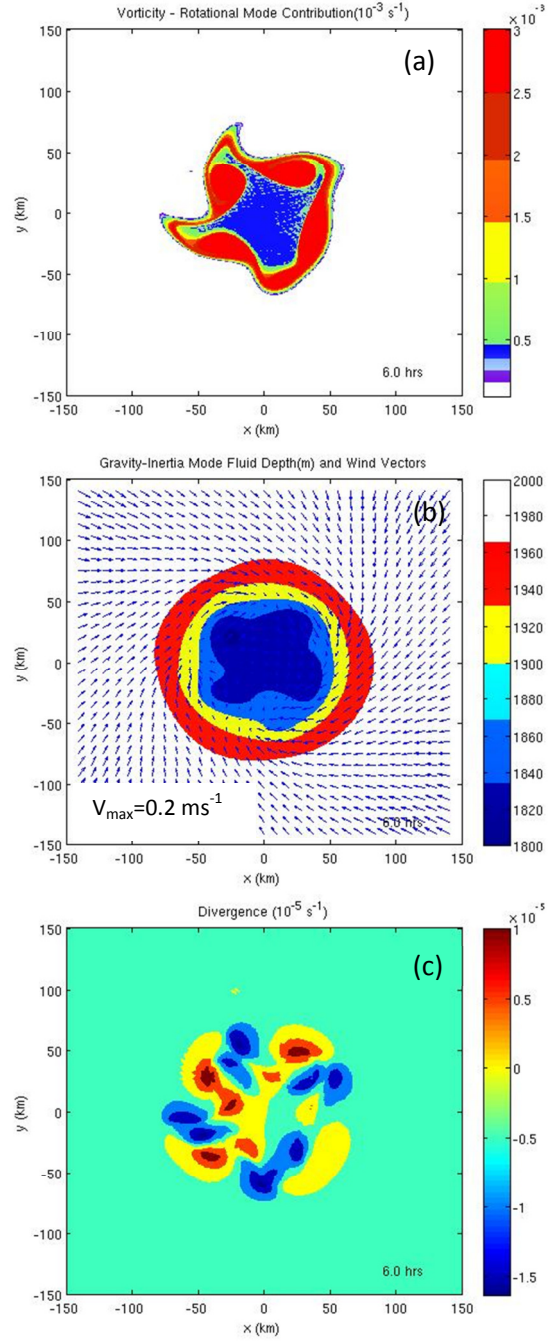


Figure 4: Various fields for the annulus case at 6 hrs. (a) Rotational mode contribution to the absolute vorticity. (b) The gravity-inertia mode contribution to the wind and fluid depth. (c) The divergence field.

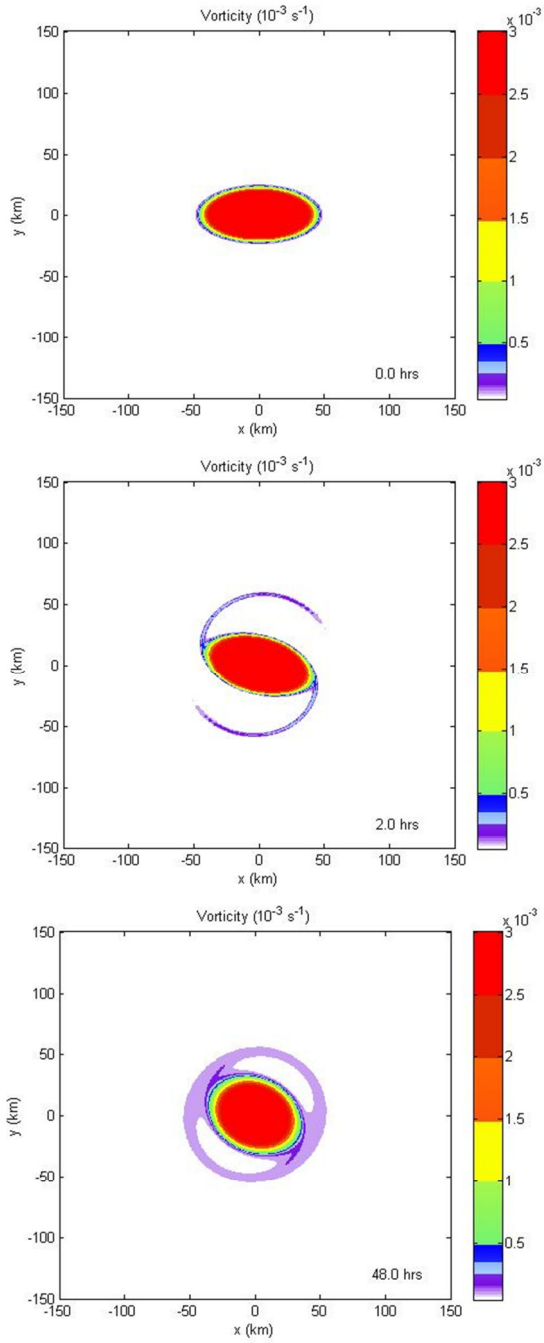


Figure 5: Evolution of an initially elliptic vortex at 0, 2, and 48 hours.

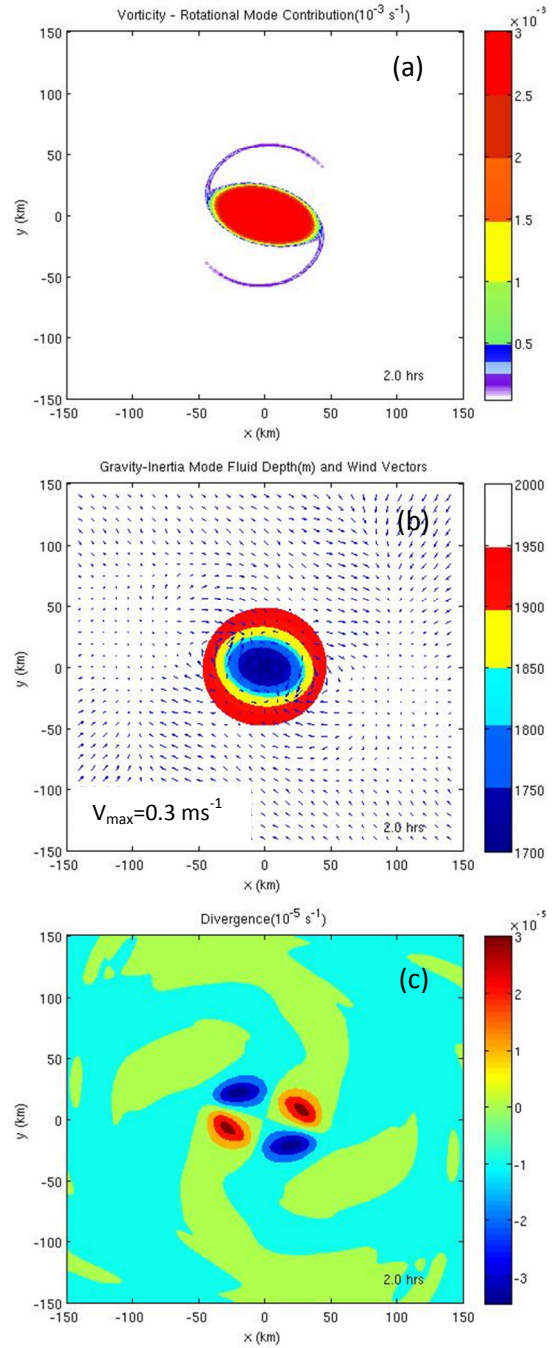


Figure 6: Various fields for the elliptical case at 2 hrs. (a) Rotational mode contribution to the absolute vorticity. (b) The gravity-inertia mode contribution to the wind and fluid depth. (c) The divergence field.